

# Decade long *RXTE* monitoring observations of Be/X-ray binary pulsar EXO 2030+375

Prahlad Epili<sup>\*</sup>, Sachindra Naik<sup>†</sup>, Gaurava K. Jaisawal<sup>‡</sup> and Shivangi Gupta<sup>§</sup>  
*Astronomy and Astrophysics Division, Physical Research Laboratory, Navrangapura, Ahmedabad - 380009, Gujarat, India*

## ABSTRACT

We present a comprehensive timing and spectral studies of Be/X-ray binary pulsar EXO 2030+375 using extensive *Rossi X-ray Timing Explorer* observations from 1995 till 2011, covering numerous Type I and 2006 Type II outbursts. Pulse profiles of the pulsar were found to be strongly luminosity dependent. At low luminosity, the pulse profile consisted of a main peak and a minor peak that evolved into a broad structure at high luminosity with a significant phase shift. A narrow and sharp absorption dip, also dependent on energy and luminosity, was detected in the pulse profile. Comparison of pulse profiles showed that the features at a particular luminosity are independent of type of X-ray outbursts. This indicates that the emission geometry is solely a function of mass accretion rate. The broadband energy spectrum was described with a partial covering high energy cutoff model as well as a physical model based on thermal and bulk Comptonization in accretion column. We did not find any signature of cyclotron resonance scattering feature in the spectra obtained from all the observations. A detailed analysis of spectral parameters showed that, depending on source luminosity, the power-law photon index was distributed in three distinct regions. It suggests the phases of spectral transition from sub-critical to super-critical regimes in the pulsar as proposed theoretically. A region with constant photon index was also observed in  $\sim(2-4)\times 10^{37}$  erg s<sup>-1</sup> range, indicating critical luminosity regime in EXO 2030+375.

**Key words:** stars: neutron – pulsars: individual: EXO 2030+375 – X-rays: stars.

## 1 INTRODUCTION

Most of the accretion powered binary X-ray pulsars are among the brightest sources in our Galaxy. They belong to the class of high mass X-ray binaries in which a neutron star accretes matter from a massive  $>10 M_{\odot}$  main-sequence companion. Depending on the evolutionary state of the donor, mass transfer from the companion star to the compact object takes place through capture of stellar wind or accretion from a huge circumstellar disk around the companion star (Paul & Naik 2011). Among confirmed high mass X-ray binaries (HMXBs), Be/X-ray binaries (BeXBs) represent about two-third population with neutron star as the compact object. The optical companion in these systems is a non-supergiant B or O type star that shows emission lines in its spectrum (Reig 2011). An excess emission in the infrared band is also observed from these companion stars in BeXBs. It is believed that due to rapid rotation, the Be star

expels material equatorially forming a huge disk, called as circumstellar disk, around it. The observed emission lines and infrared excess in the spectrum are attributed to the presence of circumstellar disk around the central Be star.

A neutron star in BeXBs revolves in a wide and moderate eccentric orbit. While passing close to the periastron, an abrupt mass accretion from the circumstellar envelope onto the neutron star gives rise to strong X-ray outbursts. The intensity during such outbursts increases up to an order of magnitude than the quiescent phase. BeXBs generally show periodic or normal (Type I) X-ray outbursts that occur at the periastron passage of the neutron star. These outbursts cover a small fraction of the orbit ( $<20-30\%$ ) and last for a few days to weeks (Stella, White & Rosner 1986). Another class of X-ray outbursts such as giant outbursts (Type II) are also seen from the neutron stars in BeXBs. These outbursts cover a significant fraction or multiple orbits lasting for several weeks to months. Type II X-ray outbursts are quite rare and independent of the orbital phase or periastron passage of the binary. During normal and giant X-ray outbursts, the luminosity of the pulsar generally reaches up to  $\leq 10^{37}$  and  $10^{38}$  erg s<sup>-1</sup>, respectively (Okazaki & Negueruela 2001).

\* E-mail: prahlad@prl.res.in

† snaik@prl.res.in

‡ gaurava@prl.res.in

§ shivangi@prl.res.in

The spin period of BeXB pulsars ranges from a few seconds to about thousand seconds. During outbursts, change in spin period of the pulsars has also been observed. This occurs because of torque transfer from accreting material to the neutron star. Accretion powered pulsars usually show broadband emission ranging from soft to hard X-rays. It is interpreted as due to thermal or bulk Comptonization of seed photons from the hot spots on the neutron star surface across the accretion column (Becker & Wolff 2007). Apart from the continuum, the energy spectrum of pulsars also shows the presence of several other components such as soft X-ray excess, iron fluorescence emissions, cyclotron resonance scattering features (CRSF) etc. Detection of CRSFs in the pulsar spectrum provides a direct and most accurate method for the estimation of surface magnetic field of neutron stars. These features are originated due to the resonant scattering of photons with electrons in quantized energy levels in the presence of strong magnetic field. Spectrum and pulse profile (representation of beam function) of the pulsars can change depending on the mass accretion rate, accretion geometry and physical processes occurring close to the neutron star. For a detailed description on the properties of transient HMXB pulsars, refer to articles by Paul & Naik (2011) and Caballero & Wilms (2012).

Be/X-ray binary pulsar EXO 2030+375 was discovered during a giant X-ray outburst in 1985, with *EXOSAT* observatory (Parmar, White & Stella 1989b). The observations during the same outburst revealed the pulsating nature of the neutron star with a spin period of 42 s along with an orbital modulation of 44.3–48.6 days. The transient nature of the pulsar was revealed during these observations. The 1–20 keV luminosity of the pulsar was observed to change by a factor of  $\geq 2500$  from quiescence over a duration of 100 days. A significant spin-up ( $-P/\dot{P} \sim 30$  yr) of the pulsar was also observed during the *EXOSAT* observations (Parmar, White & Stella 1989b), suggesting the presence of an accretion disk. Using optical and infrared observations, the counterpart of compact object was discovered as a highly reddened B0 Ve star located at a distance of 7.1 kpc (Motch & Janot-Pacheco 1987; Coe 1988; Wilson et al. 2002). Stollberg (1997) derived orbital parameters of the binary system by using long term *BATSE* monitoring data. The orbital period was determined more precisely and found to be 46 days. Strong luminosity dependent pulse profile was seen during the 1985 outburst (Parmar et al. 1989a). At higher luminosity, the pulse profile of the pulsar was characterized by two peaks (main peak and a minor peak) separated by a phase difference of  $\sim 0.5$ . The strength of these two peaks was found to alter when the source luminosity decreased by a factor of  $\sim 100$ . This observed change in strength and structure of each of the peaks in the pulse profile with luminosity was attributed to the change in the emission beam pattern e.g. from fan beam to pencil beam geometry (Parmar, White & Stella 1989b).

EXO 2030+375 is a unique BeXB pulsar which shows regular Type I X-ray outbursts at the periastron passage (Wilson et al. 2002). At the peak of the Type I outbursts observed with the *RXTE* in 1996–2006, source flux was approximately 100 mCrab. A correlation between the spin frequency and luminosity indicated that the pulsar was spinning-up during brighter outbursts in 1992–1994. On the other hand, a spin-down trend was observed during

low luminous outbursts in 1994–2002 (Wilson et al. 2002; Wilson, Fabregatet & Coburn 2005). EXO 2030+375 was caught into a giant outburst in June 2006 with source flux peaking up to  $\sim 750$  mCrab (Krimm et al. 2006). During this giant outburst which lasted for about 140 days, the neutron star showed a remarkable spin-up behaviour (Wilson, Finger & Camero-Arranz 2008). After this outburst, many intense Type I outbursts ( $\leq 300$  mCrab) were detected for a number of orbits till the source settled to its regular mode. Since early 2015, however, the pulsar had undergone to a period of low activity for more than a year. The peak flux drastically went down during this phase and hardly any X-ray enhancement was seen at the expected periastron epochs (Fuerst et al. 2016). Recent observations with *Swift*/XRT and *NuSTAR* after March 2016, however, confirmed the recurrence of X-ray activity (Type I X-ray outbursts) along with spin-down trend in the neutron star (Kretschmar et al. 2016).

The energy spectrum of pulsar obtained from the 1985 giant outburst was described by a power-law model along with thermal blackbody component at 1.1 keV (Sun et al. 1994 and reference therein). However, an absorbed power-law modified with high energy cutoff model was widely used in later observations of EXO 2030+375 during Type I and Type II outbursts (Reig & Coe 1999; Wilson, Finger & Camero-Arranz 2008). Apart from the 6.4 keV iron fluorescence emission line, detection of cyclotron absorption line was reported at three different energies such as  $\sim 11$ , 36 and 63 keV in pulsar spectra obtained from *RXTE* and *INTEGRAL* observations during different X-ray outbursts (Reig & Coe 1999; Wilson, Finger & Camero-Arranz 2008; Klochkov et al. 2008). However, *Suzaku* observations during 2007 May–June and 2012 May Type I outbursts did not confirm the presence of any such features in the pulsar spectrum (Naik et al. 2013; Naik & Jaisawal 2015). Above *Suzaku* observations also showed some other interesting aspects. Along with iron lines, several emission lines were also detected in the spectrum. It was the first time when an absorption dip was detected in the pulse profile up to as high as  $\sim 70$  keV (Naik et al. 2013). This was explained as due to the presence of additional dense matter (partial absorber) at certain phases of the pulsar. A peculiar narrow absorption dip was also detected in soft X-ray pulse profile obtained from *XMM-Newton* observation in May 2014 at a luminosity of  $\sim 10^{36}$  erg s $^{-1}$  (Ferrigno et al. 2016). This feature was interpreted as the effect of self absorption from accretion mount onto the neutron star surface.

In this paper, we present a detailed study of decade long *RXTE* monitoring observations of the pulsar over a wide range of luminosity. Investigations on the pulse profiles and corresponding spectral parameters were performed to understand the properties of the pulsar during Type I and Type II outbursts. Along with standard continuum models used to describe the pulsar spectrum, we also used a physical model based on thermal & bulk Comptonization of infalling plasma in the accretion column (BW model; Becker & Wolff 2007; Ferrigno et al. 2009) to describe the spectrum of EXO 2030+375. We have used this model to understand the physical properties of accretion column across a wide range of the pulsar luminosity. Section 2 describes the details of observations and data analysis procedures for

**Table 1.** Log of *RXTE*/PCA observations of the pulsar EXO 2030+375 during Type I and Type II outbursts.

Year of Observations	Proposal ID	No. of Obs. (IDs)	Time range (MJD)	On Source time (ksec)
1996 Jul	P10163	18	50266.55 – 50274.56	67.42
1998 Jan	P30104	2	50825.02 – 50827.77	37.94
2002 Jun	P70074	21	52431.97 – 52441.47	76.91
2003 Sep	P80071	15	52894.44 – 52898.32	145.87
2005 Jun – 2006 Feb	P91089	52	53540.78 – 53776.28	145.57
2006 Mar – 2006 Nov	P92067, P91089, P92066	143	53816.96 – 54069.97	342.34
2006 Dec – 2007 Jun	P92422	147	54070.95 – 54279.51	221.91
2007 Jun – 2008 Oct	P93098	79	54280.56 – 54749.53	202.41
2008 Dec – 2009 Oct	P94098	40	54830.20 – 55114.49	92.55
2010 Jan – 2010 Nov	P95098	43	55197.87 – 55530.08	83.79
2011 Jan – 2011 Nov	P96098	46	55566.06 – 55895.74	106.68

*RXTE* and *NuSTAR* observations. We present the results obtained from timing and spectral studies in Section 3. The implication of our results are discussed in Section 4.

## 2 OBSERVATIONS AND ANALYSIS

EXO 2030+375 has been observed numerous times during *RXTE* era i.e. between 1995-2012. These observations were performed at multiple epochs during 2006 Type II and several Type I outbursts. We have analyzed a total of 606 pointing observations for an effective exposure of 1.52 million seconds in the present study to understand timing and spectral properties of the pulsar over a span of 15 years. A detail log of relevant observations are given in Table 1. A *Nuclear Spectroscopic Telescope Array* (*NuSTAR*) observation of the pulsar performed during an extended period of low activity in 2015 is also used in our work.

### 2.1 *RXTE*

Space based X-ray observatory *RXTE* was launched on 1995 December 30 in a low earth orbit for understanding the physics and dynamics of compact objects. It carried highly timing and moderate spectral capability instruments such as Proportional Counter array (PCA; [Jahoda et al. 1996](#)) and High Energy Timing Experiment (HEXTE; [Rothschild et al. 1998](#)), sensitive in the soft to hard X-rays. The all sky monitor (ASM; [Levine et al. 1996](#)), effective in 1.5-12 keV range was also the essential part of the observatory. The PCA detector of *RXTE* consisted of an array of five identical Proportional Counter Units (PCUs) with a total collecting area of  $\sim 6500$  cm<sup>2</sup>. The individual PCUs had three Xenon layers having two anode chains in each of them. Each PCU was sensitive in 2-60 keV range and had a field of view of 1 deg FWHM ([Jahoda et al. 2006](#)). Including the Xenon-filled main counter, the detector also had a Propane “veto” layer on either sides with aluminized Mylar window for background rejection. The hard X-ray unit of *RXTE*, HEXTE consisted of two main clusters A and B, rocking orthogonally to provide simultaneous measurement of source and background. Each cluster was made of

four NaI(Tl)/CsI(Na) phoswich scintillation detectors working in 15–250 keV range. The total collecting area of both the clusters was  $\sim 1600$  cm<sup>2</sup>.

For our analysis, we have utilized publicly available *RXTE* observations acquired from 1996 July to 2011 November carried out during various Type I and Type II X-ray outbursts (see Table 1). We have mainly used the PCA standard-1 and standard-2 binned mode data for timing and spectral studies of the pulsar, respectively. For processing, standard methods are followed by creating appropriate good time interval file and filter selection on all available PCUs using HEASoft (version 6.16) package. The source light curves were extracted in the 2-60 keV from standard-1 data at 0.125 s time resolution using *saextract* task of FTOOLS. Using *runpcabackest* command, the corresponding background light curves were generated from standard-2 data by using the bright background model provided by instrumentation team. Source and background spectra were extracted from standard-2 data by using *saextract* task for all these observations. The response matrices were created for each of the observations by using *pcarsp* task. In addition to PCA, the HEXTE data were also analyzed to get hard X-ray spectrum from cluster-B for the observations carried out during 2006 giant outburst. Standard procedures were followed to extract source and background spectra and corresponding response matrices. Dead-time correction was also applied on the HEXTE spectra.

### 2.2 *NuSTAR*

*NuSTAR* is the first hard X-ray imaging observatory which was launched in 2012 June ([Harrison et al. 2013](#)). It consists of two identical grazing angle focusing telescopes FPMA and FPMB, operating in the range of 3-79 keV. A target of opportunity observation (ID: 90201029002) was performed for the pulsar on 2015 July 25 for an effective exposure of  $\sim 57$  ks. Though the observation was carried out at an orbital phase where Type I X-ray outburst was expected, there was no significant X-ray activity observed in the *Swift*/BAT monitoring light curve ([Füerst et al. 2016](#)). Using NUSTARDAS software v1.4.1 of HEASoft, we have reprocessed the data and generated barycentric corrected light curves, spec-

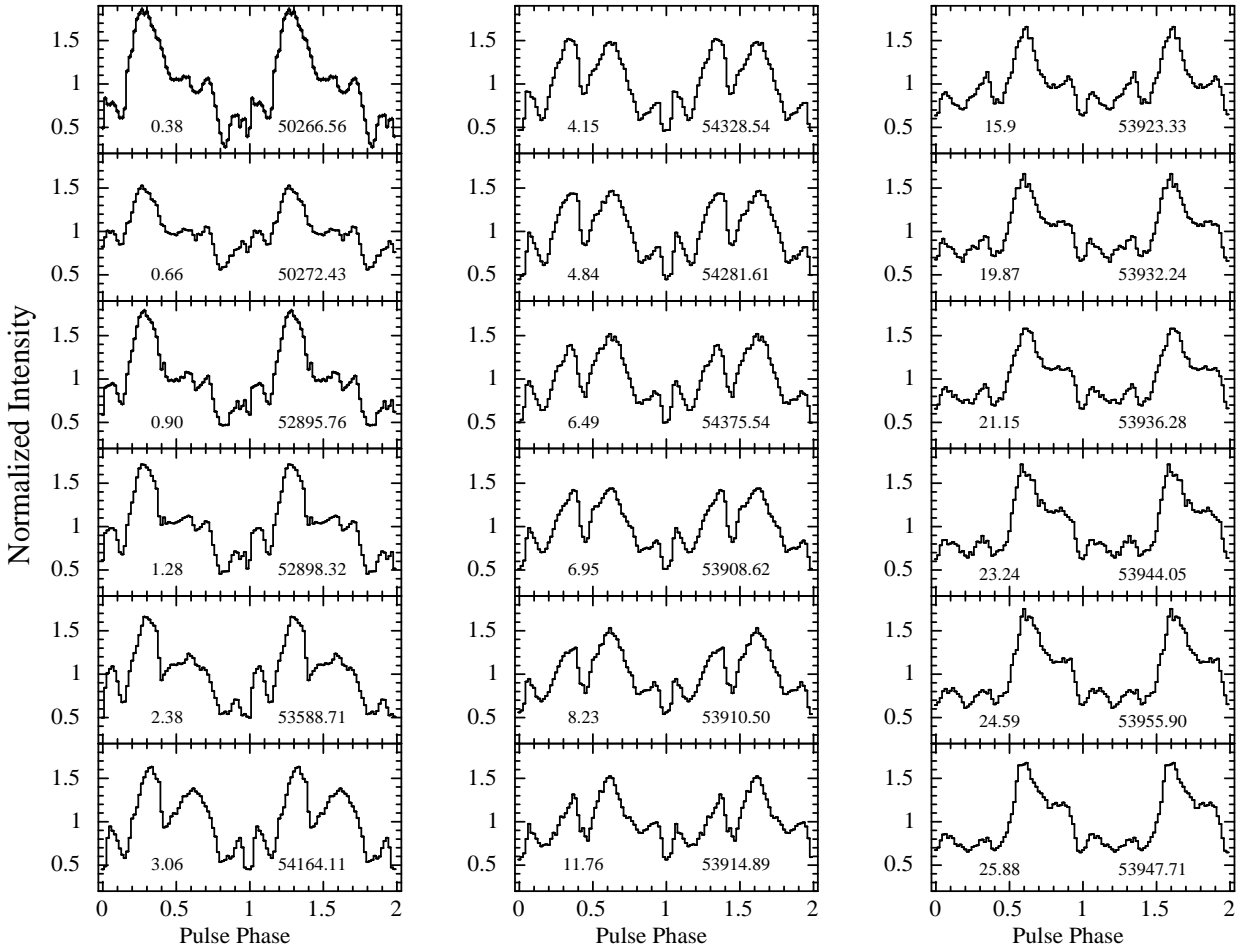


**Figure 1.** Pulse profiles of EXO 2030+375 obtained from Type I and Type II outbursts at different luminosities in 2-60 keV range. These profiles are generated by folding the *RXTE*/PCA light curves at respective pulse period estimated separately for each of the observations. The epochs used for folding the light curves with corresponding pulse period were considered close to the beginning of the observation and adjusted manually to align the pulse profiles for comparison. The numbers quoted in left and right side of each panel denote the 3-30 keV luminosity (in units of  $10^{37}$  erg  $s^{-1}$ ) and beginning of the corresponding observation (in MJD) of the pulsar, respectively. Two pulses are shown in each panel for clarity. The error bars represent  $1\sigma$  uncertainties.

tra, and response matrices and effective area files. The source products were estimated from a circular region of 120 arcsec around the central source from FPMA and FPMB event data. The background light curve and spectra were also accumulated in a similar manner by considering a circular region of 90 arcsec away from the source.

### 3 TIMING ANALYSIS

#### 3.1 Luminosity dependent pulse profiles

As described above, source and background light curves in 2-60 keV range were extracted at a time resolution of 0.125 s from *RXTE*/PCA data. The barycentric correction was applied to the background subtracted light curves by using *faxbary* task of FTOOLS. The  $\chi^2$ -maximization technique was used to estimate the spin period of the neutron star for all epochs of *RXTE* observations used in present analysis. We generated pulse profiles of the pulsar by folding the light curves at respective spin periods. The epochs used for folding were chosen close to the beginning of the observations and in such a manner that all the pulse profiles are

aligned at their minima for a better comparison. In order to understand the emission geometry, we were interested to explore the shape of pulse profiles over a wide range of source luminosity. The observations obtained from various Type I outbursts and 2006 giant outburst are used in our study. Figure 1 shows the 2-60 keV pulse profiles of the pulsar in increasing trend of luminosity, starting from  $\sim 3.8 \times 10^{36}$  to  $2.6 \times 10^{38}$  erg  $s^{-1}$ . The numbers quoted in each panel of Figure 1 represent the 3-30 keV source luminosity (in the unit of  $10^{37}$  erg  $s^{-1}$ ; first number) and the beginning of the corresponding observation (in MJD; second number). The luminosity of the source during each of the observations was calculated based on the spectral fitting (see section 4.1). It is clear from the figure that the pulse profiles are strongly dependent on source luminosity. At lower luminosity ( $\sim 10^{36}$  erg  $s^{-1}$ ), the pulse profile consisted of a significant peak at pulse phase of  $\sim 0.3$  along with a minor peak at  $\sim 0.7$  phase. Sharp dip-like features were also visible in the profiles below 0.2 phase. With increase in luminosity, the secondary minor peak starts evolving into prominence and becomes comparable to the primary peak (at  $\sim 0.3$  pulse phase) at a luminosity of  $\sim (4-7) \times 10^{37}$  erg  $s^{-1}$ . Beyond this, the second peak re-

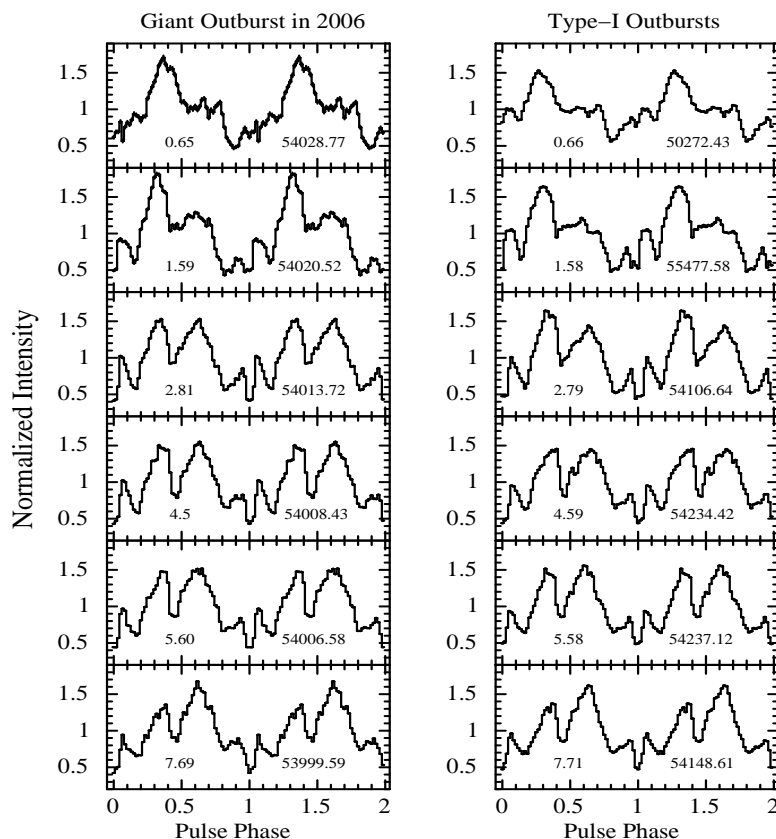


**Figure 2.** Pulse profiles of EXO 2030+375 during the Type II outburst in 2006 (left panels) and during normal Type I outbursts (right panels) in 2-60 keV range at comparable luminosities. The 3-30 keV luminosity of the pulsar (in  $10^{37}$  erg  $s^{-1}$  units) and beginning of corresponding observation (in MJD) are quoted in left and right side of each panel. Two pulses are shown in each panel for clarity. The error bars represent  $1\sigma$  uncertainties.

mains significant whereas the strength of first peak gradually decreases and finally disappears from the pulse profile at a luminosity of  $\geq 1.6 \times 10^{38}$  erg  $s^{-1}$ . Multiple absorption dips clearly appeared in the pulse profiles at certain pulse phases during the evolution with source luminosity. It is worth mentioning that the shape of pulse profiles at extreme ends of observed source luminosity (first and last panels of Figure 1) is relatively similar with a significant phase shift.

### 3.2 Pulse profiles during Type I and Type II outbursts

To investigate the changes in observed properties of the pulsar during Type I and Type II X-ray outbursts, pulse profiles at various epochs were generated and shown in Figure 2. The data from several Type I outbursts were used at appropriate flux level to compare with the observations at same intensity level, carried out during the 2006 June giant outburst. Left panels in the figure show the pulse profiles obtained from several observations during the 2006 giant outburst whereas the right panels show the profiles obtained from various Type I outbursts at comparable source luminosity. From the figure, it can be noted that (i) shape of pulse profiles are similar at comparable source intensity, irrespective of type of X-ray outbursts, (ii) evolution of pulse profiles with luminosity during both type of outbursts are also similar as remarked in Figure 1. This signifies that pulse profiles

of EXO 2030+375 are independent of the type of X-ray outbursts.

A thorough investigation of pulse profiles of the pulsar obtained from observations performed during Type II outburst was also carried out. The motivation was to probe the evolution and possible change in the emission geometry at same intensity during the rising and declining part of the 2006 giant outburst. Due to large number of pointings in 2006 June, we were able to trace the pulsar beam function at both phases of the outburst. For this, the pulse profiles were generated at luminosity ranging from  $10^{37}$  to  $10^{38}$  erg  $s^{-1}$ . Our results showed that the profiles during the rising and declining phases of the outburst are similar at comparable luminosities. This behavior was analogous to as seen in Figure 2.

### 3.3 Peculiar narrow and sharp absorption dip

We extracted a light curve with a time resolution of 0.1 s in 3-60 keV range by using *NuSTAR* observation of the pulsar. As described above, standard data reduction procedure was followed to extract the source and background light curves. From the background subtracted and barycentric corrected light curve, spin period of the pulsar was estimated by using *efsearch* task of FTOOLS and found to be 41.2932(2) s. Using this period, the pulse profile of the pulsar was generated by folding the light curve at 128 phase bins and shown in the

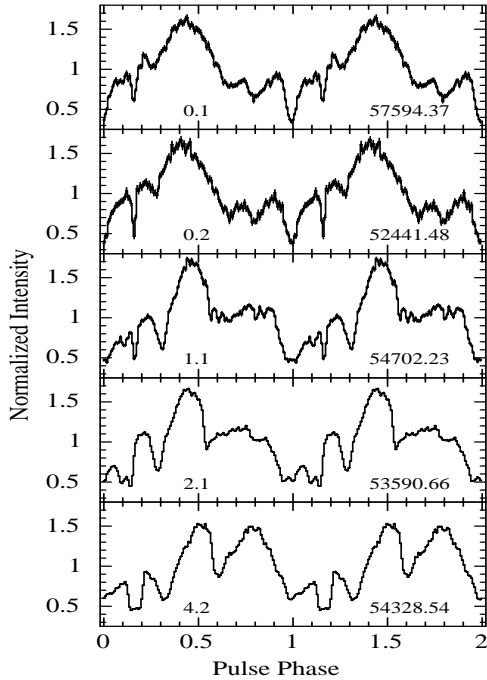


**Figure 3.** A peculiar narrow dip (in 0.1-0.2 phase range) can be seen in the pulse profiles of EXO 2030+375. The profile in top panel represents data from the *NuSTAR* observation whereas other panels show profiles obtained from the *RXTE* observations. The 3-30 keV luminosity (in unit of  $10^{37}$  erg  $s^{-1}$ ) and the beginning of corresponding observation (in MJD) are quoted in left and right sides of each panel, respectively. Two pulses are shown in each panel for clarity. The error bars represent  $1\sigma$  uncertainties.

top panel of Figure 3. Other panels of figure show the profiles from *RXTE* observations in the 2-60 keV range in increasing order of source luminosity. A narrow and sharp dip like structure in 0.1-0.2 phase range can be clearly seen in the profiles when the pulsar luminosity was  $\sim 10^{36}$  erg  $s^{-1}$  (*NuSTAR* observation). This peculiar feature was also detected in the pulse profile obtained from *XMM-Newton* observation of the pulsar during the 2014 May outburst (Ferrigno et al. 2016). Figure 3 shows that this peculiar dip is luminosity dependent and can be seen in the profiles up to the luminosity  $\leq 4 \times 10^{37}$  erg  $s^{-1}$ . Beyond this luminosity, the feature merges into a broader dip in the profile (bottom panel of Figure 3). The evolution of the peculiar feature with energy also showed strong variation that can be traced up to 30 keV by using data from *NuSTAR* observation.

## 4 SPECTRAL ANALYSIS

### 4.1 Phase-averaged spectroscopy

To probe spectral characteristics of the pulsar and corresponding changes with luminosity, we carried out spectral studies by using data from *RXTE* observations. Source and background spectra were extracted by following standard procedure as described in Section 2.1 for all the *RXTE* observations. Using appropriate background spectra and response matrices, the source spectra from PCA detector were fitted by using *XSPEC* package. Data in 3–30 keV range were used in the spectral fitting. A systematic uncertainty of 0.5%

was added to the data. While fitting the data, we explored several continuum models that are used to describe the energy spectrum of accretion powered X-ray pulsars. These models are high-energy cutoff power-law, cutoff power-law, negative and positive exponentiation cutoff power-law, and with more physical model such as CompTT. In our analysis, we used an absorbed power-law model with a high-energy cutoff to describe the continuum spectrum of the pulsar. This model has been frequently used to express the broadband spectrum of EXO 2030+375 (Reig & Coe 1999; Wilson, Finger & Camero-Arranz 2008).

It has been recently found that the continuum of Be/X-ray binary pulsars is noticeably affected by the presence of additional matter at certain pulse phases during outbursts that can't be simply explained by a single absorber (Naik et al. 2013; Jaisawal, Naik & Epili 2016). A partial covering absorption component along with the continuum model is generally used to describe the pulsar spectrum in phase-averaged as well as phase-resolved spectroscopy. In our fitting, a high energy cutoff power-law model was unable to fit the observed spectrum, specifically during bright phases of outbursts. Addition of a partial covering component improved the fitting further and yielded an acceptable value of reduced- $\chi^2$  ( $\sim 1$ ). The iron fluorescence emission line at  $\sim 6.4$  keV was also detected in the pulsar spectrum. A partially covering absorbed power law with high-energy cutoff model is mathematically expressed as

$$N(E) = e^{-N_{H1}\sigma(E)}(K_1 + K_2e^{-N_{H2}\sigma(E)}) f(E)$$

where

$$f(E) = E^{-\Gamma} \quad \text{for } E < E_c \\ = E^{-\Gamma} e^{-\left(\frac{E-E_c}{E_f}\right)} \quad \text{for } E > E_c$$

where,  $f(E)$  represents the high energy cutoff power-law model with  $\Gamma$  as the power-law photon index,  $E_c$  and  $E_f$  are the cutoff and folding energies in keV, respectively. The normalization constants  $K_1$  &  $K_2$  are in the units of photon  $\text{keV}^{-1} \text{cm}^{-2} \text{s}^{-1}$ .  $N_{H1}$  &  $N_{H2}$  are the equivalent galactic hydrogen column density and the additional column density (in units of  $10^{22}$  atoms  $\text{cm}^{-2}$ ), respectively.  $\sigma(E)$  is the photoelectric absorption cross-section. The energy spectra of EXO 2030+375 along with the best-fitting model (top panel) and residuals (bottom panel) for six epochs of *RXTE* observations are shown in Figure 4. Observation IDs and 3-30 keV pulsar luminosity during these epoch of observations are quoted in the figure. The best-fitted parameters obtained from spectral fitting of data obtained at these epochs are given in Table 2.

During 2006 June outburst, detection of a cyclotron absorption line like feature at  $\sim 11$  keV in the pulsar spectrum was reported (Wilson, Finger & Camero-Arranz 2008). We used same observation in the present study to investigate the cyclotron line feature in the pulsar spectrum. During this outburst, as the pulsar luminosity was very high, data from PCA and HEXTE detectors were used to get a broad-band spectral coverage. The 3-100 keV broad-band spectrum, obtained from the *RXTE* observation on MJD 53962.5, was fitted with a high energy cutoff power-law model yielding a poor fit with a reduced  $\chi^2$  of  $> 8$ . A broad absorption-like feature at  $\sim 10$  keV was detected in the spectral residual (panel C of Figure 5). Various combination of models such as

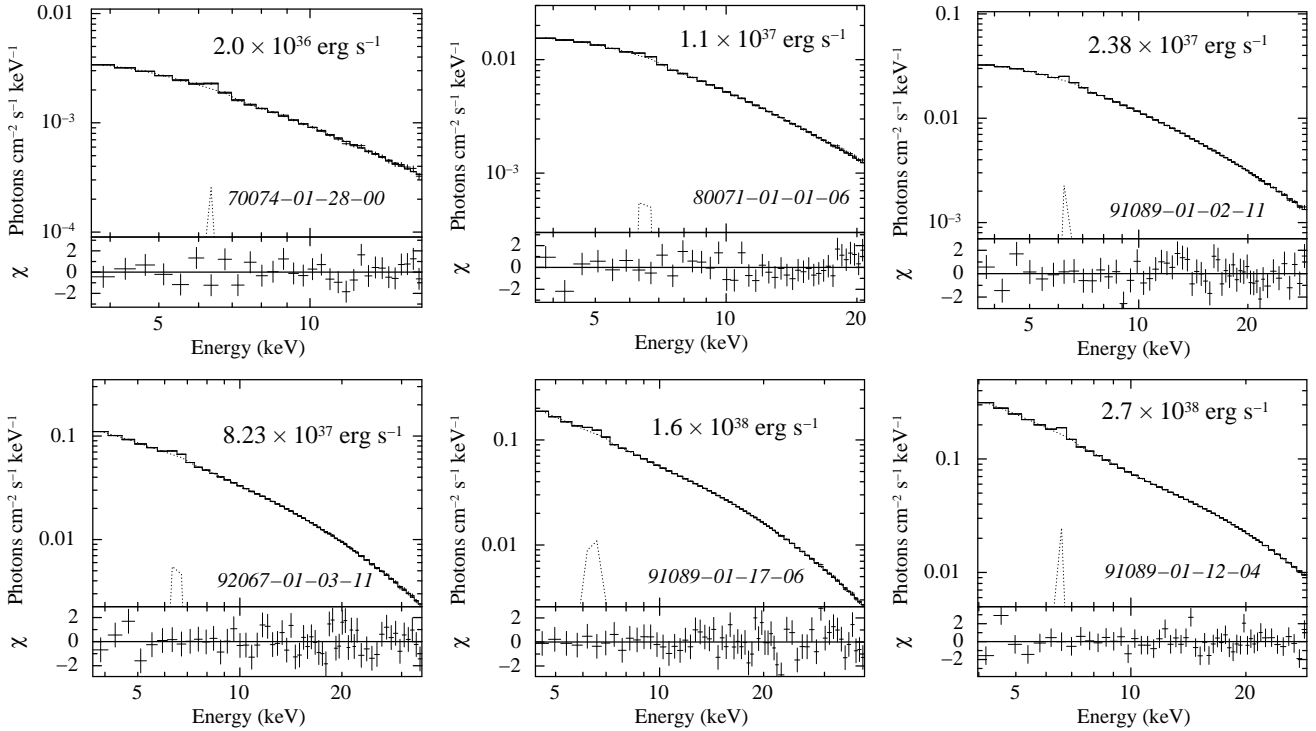


**Figure 4.** Phase-averaged energy spectra of EXO 2030+375 at different luminosity levels, obtained from six epochs of *RXTE* observations during Type I and Type II X-ray outbursts. The spectra were fitted with partial covering high energy cutoff model along with an iron emission line at  $\sim 6.4$  keV. The source spectrum and best-fit model are shown in the top panel whereas the contribution of residuals to  $\chi^2$  at each energy bin are shown in the bottom panel for each epoch of *RXTE* observations. The observation IDs (in italics) and corresponding source luminosity are quoted in the figure.

high energy cutoff power-law, CompTT, NPEX along with other components such as blackbody or a partial absorber were used to test reliability of the reported line. Addition of a partial covering component to the above continuum models resolves the broad feature with a reduced- $\chi^2$  close to 1. Therefore, a high energy cutoff model along with a partial covering component was used as best-fit model in our analysis. We generated Crab-ratio to check the presence of absorption like feature in the pulsar spectrum. The Crab-ratio is obtained by normalizing the pulsar spectrum with the feature-less power-law spectrum of Crab pulsar to remove the presence of any uncertainties related to calibration and model (see also Jaisawal, Naik & Paul 2013). This ratio showed a highly absorbed spectrum along with a 6.4 keV iron emission line below 10 keV. We did not find any signature of absorption feature in 10-20 keV range in the Crab-ratio (panel B of Figure 5). Spectral residuals obtained from fitting the pulsar spectral with different continuum models are shown in panels C, D, E and F of Figure 5. The absence of any absorption like feature in 10-20 keV range can be clearly seen in above panels. To check the presence/absence of this absorption like feature, we fitted 3-79 keV broad-band spectrum of EXO 2030+375, obtained from a *NuSTAR* observation during an extended period of low activity in 2015 with a high energy cutoff model. Any emission/absorption like features were not seen in the spectrum.

Spectral parameters such as power-law photon index, cutoff energy, folding energy, additional column density ( $N_{H2}$ ), covering fraction, hardness ratio (ratio between 10-

30 keV flux and 3-10 keV flux) obtained from spectral fitting of all *RXTE* observations of EXO 2030+375 are shown with corresponding 3-30 keV luminosity in Figure 6. All these parameters showed intriguing trends with luminosity which had not been explored earlier. In the figure, one can notice that the values of power-law photon index are distributed in three distinct regions such as negative, constant, and positive correlations with source luminosity which suggest a direct measure of spectral transition in EXO 2030+375. At lower luminosity ( $\leq 10^{37}$  erg  $s^{-1}$ ), the pulsar spectrum was relatively soft. A negative correlation between the power-law photon index and luminosity can be clearly seen for this regime. The value of photon index was found to vary between 1.2 and 1.8 (first panel of Figure 6). When the luminosity was in the range of  $2-4 \times 10^{37}$  erg  $s^{-1}$ , the distribution of values of photon index did not show any dependence on source luminosity. With increase in source luminosity, the photon index showed a positive correlation. It is, therefore, clear that the pulsar changes its spectral behavior with change in luminosity. Flux ratio (ratio between flux in 10-30 keV range and 3-10 keV range) also showed smooth transition with increase in pulsar luminosity (left bottom panel of Figure 6). As mentioned earlier, while fitting spectra from high flux level of the outbursts, a partially absorbed component was included in the fitting model. This was required in spectral fitting when the pulsar luminosity was above  $3 \times 10^{37}$  erg  $s^{-1}$ . In our spectral fitting, the maximum value of additional column density ( $N_{H2}$ ) obtained was as high as  $250 \times 10^{22}$   $cm^{-2}$  which is significantly larger than the

**Table 2.** Best-fitting spectral parameters with  $1\sigma$  errors obtained from *RXTE/PCA* observations of EXO 2030+375 at six different luminosities. The best-fit model consists of a partial covering high-energy cutoff power-law model with a Gaussian component.

Parameters	Observation IDs					
	70074-01-28-00	80071-01-01-06	91089-01-02-11	92067-01-03-11	91089-01-17-06	91089-01-12-04
$N_{H1}^a$	$5.9\pm 0.8$	$6.2\pm 0.5$	$5.2\pm 0.3$	$2.8\pm 0.5$	$1.5\pm 0.4$	$3.41\pm 0.25$
$N_{H2}^b$	–	–	–	$139.3\pm 17.5$	$166.5\pm 5.5$	$241.9\pm 4.0$
Covering fraction	–	–	–	$0.25\pm 0.02$	$0.35\pm 0.01$	$0.45\pm 0.01$
Photon Index ( $\Gamma$ )	$1.72\pm 0.06$	$1.45\pm 0.06$	$1.34\pm 0.03$	$1.43\pm 0.05$	$1.61\pm 0.02$	$1.80\pm 0.03$
$E_{cut}$ (keV)	$8.2\pm 0.8$	$7.6\pm 0.4$	$7.7\pm 0.2$	$8.0\pm 0.3$	$8.2\pm 0.2$	$7.8\pm 0.2$
$E_{fold}$ (keV)	$31.9\pm 5.6$	$23.3\pm 1.8$	$23.3\pm 0.8$	$21.2\pm 0.9$	$23.5\pm 0.5$	$25.7\pm 0.8$
<i>Emission lines</i>						
Fe $K\alpha$ line energy (keV)	$6.32\pm 0.16$	$6.50\pm 0.11$	$6.33\pm 0.05$	$6.51\pm 0.08$	$6.43\pm 0.03$	$6.52\pm 0.04$
Width of Fe line (keV)	0.1	0.1	0.1	0.15	$0.31\pm 0.07$	0.1
Source flux						
Flux <sup>c</sup> (3-10 keV)	$0.17\pm 0.03$	$0.88\pm 0.09$	$1.8\pm 0.9$	$6.6\pm 0.7$	$13.8\pm 0.7$	$25.0\pm 1.5$
Flux <sup>c</sup> (10-30 keV)	$0.16\pm 0.02$	$0.94\pm 0.10$	$2.2\pm 0.1$	$7.1\pm 0.8$	$12.7\pm 0.6$	$19.4\pm 1.2$
Flux <sup>c</sup> (3-30 keV)	$0.33\pm 0.04$	$1.82\pm 0.19$	$4.0\pm 0.20$	$13.7\pm 1.4$	$26.5\pm 1.3$	$44.4\pm 2.6$
Source Luminosity						
$L_X^d$ (3-30 keV)	$0.20\pm 0.03$	$1.10\pm 0.12$	$2.38\pm 0.14$	$8.23\pm 0.89$	$15.96\pm 0.90$	$26.77\pm 1.72$
Reduced $\chi^2$ ( <i>d.o.f</i> )	0.99 (24)	1.01 (34)	1.04 (46)	1.00 (50)	1.08 (53)	1.11 (43)

Notes: <sup>a</sup> : Equivalent hydrogen column density (in  $10^{22}$  atoms  $\text{cm}^{-2}$  unit); <sup>b</sup> : Additional hydrogen column density (in  $10^{22}$  atoms  $\text{cm}^{-2}$  unit); <sup>c</sup> : Absorption corrected flux in unit of  $10^{-9}$  ergs  $\text{cm}^{-2}$   $\text{s}^{-1}$ ; <sup>d</sup> : The 3-30 keV X-ray luminosity in the units of  $10^{37}$  ergs  $\text{s}^{-1}$  assuming a distance of 7.1 kpc to the source.

value of interstellar absorption column density in the source direction. From our fitting, the values of additional column density and covering fraction were found to be strongly luminosity dependent (middle panels of Figure 6). The cut-off energy and folding energy did not show any noticeable changes with the pulsar luminosity (last panels of Figure 6). The parameters obtained from *NuSTAR* observation are also included in the figure.

#### 4.2 A physical model to describe the pulsar continuum spectrum

To explore the physical properties of accretion column, we have fitted the Becker & Wolff (BW) model with the phase averaged spectra of the pulsar. This model is proposed by Becker & Wolff (2007) to explain the emission from accretion powered X-ray pulsars by considering the effects of thermal and bulk Comptonizations in accretion column. It has been successful in explaining the broadband spectra of bright X-ray pulsars such as 4U 0115+63 (Ferrigno et al. 2009), 4U 1626-67 (D’Ai et al. 2017), Her X-1 (Wolff et al. 2016). According to this model, seed photons originated due to bremsstrahlung, blackbody and cyclotron emissions undergo thermal and bulk Comptonization in the accretion column. Comptonization of these seed photons with highly energetic electrons lead to the power-law like resultant spectra with high energy exponential cutoff.

Using this model, we have described the 3-70 keV broadband phase-averaged spectra of EXO 2030+375 at 23 different luminosity epochs, covering the range of  $10^{36}$ – $10^{38}$  erg  $\text{s}^{-1}$ . For a canonical neutron star mass and radius,

the BW model has six free parameters, i.e. the diffusion parameter  $\xi$ , the ratio of bulk to thermal Comptonization  $\delta$ , the column radius  $r_0$ , mass accretion rate  $\dot{M}$ , electron temperature  $T_e$  and the magnetic field strength  $B$ . Among these parameters, the mass accretion rate  $\dot{M}$  was estimated by using the observed source flux obtained from high energy cutoff empirical model and considering a source distance of 7.1 kpc (Wilson et al. 2002). Since the column radius strongly depends on accretion rate (see eq. 112 of Becker & Wolff 2007), the parameter  $\dot{M}$  was fixed at a given value while fitting the spectra. After fitting, the column radius was also fixed for getting better constraints on other spectral parameters. This was done carefully by analyzing the 2-D contour plots between  $r_0$  &  $\dot{M}$ , as similar to Ferrigno et al. (2009). The other BW model components such as normalizations of Bremsstrahlung, cyclotron and blackbody seed photons were also kept fixed as suggested in the BW\_cookbook<sup>1</sup>. A partial covering component as required in empirical models was also needed to explain the absorbed spectra of the pulsars during bright outbursts. The values of additional column density and covering fraction obtained from BW model were found to be consistent with the values obtained with the high energy cutoff power-law model. Therefore, we have not discussed these parameters in this section. An iron fluorescence line at  $\sim 6.4$  keV was also added in the continuum. Spectral parameters obtained after best fitting the pulsar spectra with BW model are given in Table 3. The values of reduced  $\chi^2$  obtained from our fitting, as given in Table 3,

<sup>1</sup> [http://www.isdc.unige.ch/~ferrigno/images/Documents/BW\\_distribution](http://www.isdc.unige.ch/~ferrigno/images/Documents/BW_distribution)



**Table 3.** Best-fitting spectral parameters with  $1\sigma$  errors obtained from *RXTE/PCA* and *RXTE/HEXTE* observations of EXO 2030+375 with BW model.

Obs-Ids	BW model Parameters							
	Luminosity <sup>a</sup> ( $10^{37}$ ergs s <sup>-1</sup> )	$\dot{M}$ ( $10^{17}$ g s <sup>-1</sup> )	$\xi$	$\delta$	B ( $10^{12}$ ) G	T <sub>e</sub> (keV)	r <sub>0</sub> (m)	Reduced $\chi^2$ (dof)
91089-01-12-04 <sup>‡</sup>	28.04 ± 0.84	14.96	1.88 ± 0.03	14.38 ± 1.01	4.25 ± 0.20	3.95 ± 0.11	177.0	1.22(103)
91089-01-12-05	28.22 ± 0.38	14.82	1.77 ± 0.02	17.57 ± 1.20	4.23	3.42 ± 0.10	165.0	1.04(80)
91089-01-15-00	27.12 ± 0.53	14.59	1.82 ± 0.02	16.82 ± 1.19	4.58	3.83 ± 0.10	158.0	1.05(104)
91089-01-14-03	26.36 ± 0.49	13.88	1.86 ± 0.03	17.03 ± 2.50	4.34 ± 0.25	4.01 ± 0.16	141.0	1.02(85)
91089-01-09-03	19.39 ± 0.39	10.44	1.98 ± 0.03	11.24 ± 0.91	4.66 ± 0.22	4.53 ± 0.12	138.0	1.09(105)
91089-01-09-00	17.11 ± 0.65	9.21	2.06 ± 0.05	9.64 ± 2.75	5.29	5.15 ± 0.40	116.0	1.09(104)
91089-01-08-01	13.40 ± 0.48	7.22	2.13 ± 0.05	10.48 ± 1.10	5.59	5.61 ± 0.14	105.0	1.08(107)
91089-01-07-00	11.63 ± 0.58	6.26	2.43 ± 0.17	4.22 ± 0.72	4.85 ± 0.35	5.56 ± 0.31	98.5	1.13(98)
92067-01-03-13	10.09 ± 0.54	5.43	2.44 ± 0.16	4.17 ± 0.54	5.18 ± 0.36	5.97 ± 0.40	74.0	1.09(90)
92067-01-03-11	8.17 ± 0.98	4.40	2.36 ± 0.29	4.30 ± 1.16	5.33 ± 0.35	6.14 ± 0.43	35.6	1.16(95)
92067-01-03-00	6.86 ± 1.47	3.69	3.11 ± 0.73	2.09 ± 1.07	5.03	6.32 ± 0.16	28.2	1.10(99)
93098-01-03-05	5.72 ± 0.70	3.25	1.91 ± 0.16	7.90 ± 1.38	4.85	4.85 ± 0.41	26.0	1.08(87)
93098-01-01-01	4.86 ± 0.46	2.79	2.08 ± 0.15	5.50 ± 1.10	4.35 ± 0.21	4.88 ± 0.27	25.5	1.05(111)
92422-01-25-06 <sup>‡</sup>	4.74 ± 0.74	2.66	3.01 ± 1.19	2.43 ± 1.20	5.39 ± 0.45	6.68 ± 0.36	24.5	1.11(101)
93098-01-01-00	3.90 ± 0.83	2.34	5.08 ± 1.24	0.97 ± 0.35	4.78	6.32 ± 0.07	19.6	1.08(102)
92422-01-05-04	3.82 ± 0.84	2.22	7.37 ± 3.18	0.64 ± 0.21	4.82	6.53 ± 0.05	19.2	0.99(96)
93098-01-02-04	3.71 ± 1.08	1.98	7.26 ± 2.86	0.62 ± 0.27	4.70	6.34 ± 0.07	23.4	1.03(89)
92422-01-14-03	3.07 ± 0.75	1.74	6.11 ± 1.95	0.77 ± 0.29	4.50	6.09 ± 0.07	17.5	1.07(90)
80071-01-01-11	1.41 ± 0.01	0.81	6.49 ± 1.05	0.66 ± 0.13	3.74	5.24 ± 0.02	17.5	1.06(87)
80071-01-01-06	1.20 ± 0.01	0.67	8.15 ± 2.50	0.52 ± 0.20	3.77	5.29 ± 0.03	16.0	1.08(86)
80071-01-01-00	1.14 ± 0.01	0.64	7.11 ± 1.65	0.60 ± 0.17	4.02	5.69 ± 0.03	18.4	1.19(97)
80071-01-01-01 <sup>‡</sup>	0.88 ± 0.01	0.48	7.89 ± 1.80	0.57 ± 0.15	3.75	5.32 ± 0.02	17.4	1.12(87)
80071-01-01-020	0.92 ± 0.01	0.44	10.29 ± 2.58	0.39 ± 0.16	3.69	5.28 ± 0.01	15.0	1.03(72)

Notes: <sup>a</sup> : The 3-70 keV luminosity in the units of  $10^{37}$  ergs s<sup>-1</sup> by assuming a distance of 7.1 kpc.

<sup>‡</sup>: indicates the observation ids from which extracted spectra are shown in Figure 7.

showed that the BW continuum model fits the data well in a wide luminosity range. For three different values of pulsar luminosity, broadband energy spectra of the pulsar from PCA and HEXTE detectors, along with best-fitted BW continuum model and Gaussian function for iron emission line are presented in top panels of the Figure 7. The bottom panels in this figure show corresponding spectral residuals of best fitted model. It can be seen that the residuals obtained from fitting the pulsar spectra with BW model did not show any evidence of presence of absorption like feature. This finding also supports the non-detection of cyclotron line in EXO 2030+375, as discussed in the above section of the paper.

Luminosity dependent variations in the parameters obtained after fitting the pulsar spectra with BW model are shown in Figure 8. An interesting trend of parameter  $\delta$  with luminosity was noticed in the third panel of the figure. This parameter signifies the ratio of bulk to thermal Comptonization occurring in the accretion column. The value of  $\delta$  was found close to unity at luminosity  $\leq 3-4 \times 10^{37}$  ergs s<sup>-1</sup>. This indicates that the effects of thermal and bulk Comptonization are nearly same in accretion column at lower luminosity of the pulsar. However, as the luminosity increases, bulk Comptonization starts playing a major role to column emissions and dominates over by a factor of 20 times as observed at lower luminosity. The column radii  $r_0$  was found to strongly dependent on luminosity or mass accretion rate.

Moreover, the diffusion parameter  $\xi$  was also observed to vary with source intensity, showing a minimum value at higher luminosity. In addition to these, the electron plasma temperature was changing in the range of 3 to 7 keV. The temperature showed a gradual increase up to luminosity  $4 \times 10^{37}$  ergs s<sup>-1</sup>. Beyond this, a cooling of plasma temperature was observed. This may occur in the presence of strong radiation dominated accretion shock at which the infalling matter mostly bulk Comptonize the seed photons that carries plasma energy by diffusing through the side walls of accretion column. It leads to the settling of plasma in accretion column at lower temperature. This model also provides an opportunity to constrain the magnetic field of the pulsar in the range of  $\sim 4-6 \times 10^{12}$  G (see Figure 8). In some cases, magnetic field estimated from this model was found insensitive to upper value, though their lower estimate was easily constrained in all these observations. Therefore, only best fitted values without error bars are quoted in Table 3.

## 5 DISCUSSION

Be/X-ray binaries show two types of X-ray outbursts such as Type I and Type II outbursts. These outbursts are known to be due to capture of huge amount of matter by the neutron star from the circumstellar disk of the companion Be star at periastron passage (Type I) or due to evacuation/truncation

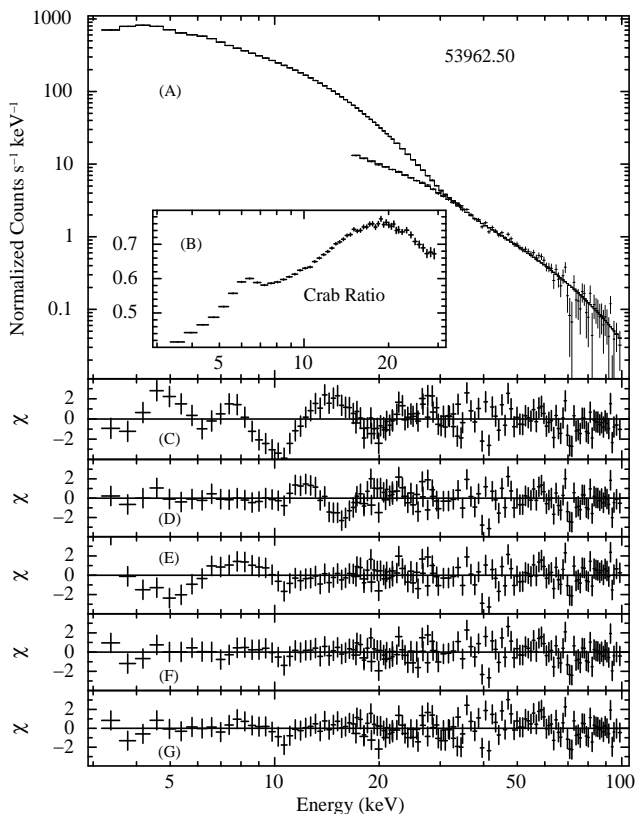


**Figure 5.** The 3-100 keV energy spectra of EXO 2030+375 obtained from PCA and HEXTE detectors of *RXTE* at the peak of 2006 giant outburst (MJD 53962.50). Source spectra along with the best fitting model e.g. a partial covering high energy cutoff model along with a Gaussian for iron emission line (panel A) and corresponding spectral residual (panel G) are shown. Panels C, D, E and F indicate the spectral residuals obtained by fitting pulsar spectra with a (i) high energy cutoff model, (ii) high energy cutoff model with a blackbody, (iii) CompTT with a blackbody, and (iv) a partial covering CompTT model with blackbody component, respectively, along with interstellar absorption component and a Gaussian function for iron emission line at 6.4 keV. Any signature of cyclotron absorption line at previously reported value of  $\sim 11$  keV is not seen in the spectral residuals. The Crab-ratio (panel B) also did not show any such feature in 10-20 keV range.

of Be circumstellar disk (Type II). During these episodes, X-ray emission from the neutron star gets transiently enhanced by a factor of ten or more. Normal (Type I) outbursts are found to be less luminous ( $10^{36-37}$  erg  $s^{-1}$ ) whereas during giant (Type II) outbursts, the luminosity reaches close to or above the Eddington luminosity of a neutron star (Negueruela et al. 1998). EXO 2030+375 is a unique Be/X-ray binary system that displays Type I outbursts almost at each periastron passage. However, the pulsar showed Type II outbursts only twice (in 1985 and 2006) since its discovery. Type I outbursts are short lived, covering about 20-30% of orbital period in contrast to giant outbursts which lasted for more than 3 months in both the occasions. The peak luminosity during normal outburst varies depending on the evolutionary state of the Be circumstellar disk. It is believed that the neutron star accretes matter from the circumstellar disk at the periastron passage and gives rise to Type I X-ray outbursts. As the Type II X-ray outbursts are

very rare, the origin for Type II outburst remains unclear. It is thought that dramatic expansion of the circumstellar disk around the Be star or instabilities in the circumstellar disk leads to such major events (Okazaki & Negueruela 2001; Reig 2011). Several analytical and numerical studies have been performed to understand the behavior of transient accretion by considering a misalignment between the orbital plane and the eccentric warped Be circumstellar disk (Okazaki, Hayasaki & Moritani 2013; Martin et al. 2014). These studies showed that accretion time scales longer than the orbital period and higher luminosity as observed during Type II outbursts are possible in such scenario. Using large number of *RXTE* observations of EXO 2030+375 during Type I and Type II outbursts, we have explored the evolution of pulse profile and its characteristics as a function of luminosity as well as type and phase of outbursts. The changes in spectral properties and its transition are also studied in detail in the paper.

### 5.1 Pulse profiles

Pulse profiles of Be/X-ray binary pulsars are generally complex due to the presence of multiple absorption dips at various spin phases of the pulsar. We have explored the evolution of pulse profiles of EXO 2030+375 over a wide range of luminosity, starting from  $\sim 10^{36}$  to  $10^{38}$  erg  $s^{-1}$  by using large number of *RXTE* observations of the pulsar. The profiles are found to be strongly luminosity dependent which has also been reported from previous studies (Parmar, White & Stella 1989b; Klochkov et al. 2008; Naik et al. 2013; Naik & Jaisawal 2015). One of the interesting results we obtained is that the profiles are similar in shape at identical luminosities irrespective of types and phases of outbursts. This indicates that the beam pattern of the pulsar does not depend on outburst characteristics, although distinct mechanism governs the origin of Type I and Type II outbursts. Accretion rate or luminosity is the vital factor that decide the shape of pulse profile of the pulsar. At lower luminosity ( $\leq 10^{37}$  erg  $s^{-1}$ ; sub-critical regime), the X-ray emission is believed to be originated from the hot spot along the accretion column in the form of pencil beam (Sasaki et al. 2010 and references therein). This beam geometry leads to the formation of a single peaked profile as seen in our study at lower luminosity. In presence of a radiation dominated shock at higher luminosity, the profile changes from single to double peaked. A mixture of pencil and fan beam patterns can contribute to the double peak structure of pulse profiles which is clearly seen in EXO 2030+375 in the luminosity range of  $\sim (3-12) \times 10^{37}$  erg  $s^{-1}$ . During the giant outbursts, mass accretion rate increases beyond the critical luminosity that shifts the height of radiative shock in the accretion column. As a result, accreted matter is obstructed by dominating radiation pressure above the shock (Becker & Wolff 2007). The photons beyond this point mostly diffuses through the side wall of the accretion column, forming a fan-beam geometry (Klochkov et al. 2008). Therefore, at higher luminosity ( $> 1.2 \times 10^{38}$  erg  $s^{-1}$ ), the pulse profiles of the pulsar could be purely due to the fan beam pattern.

The energy dependent pulse profiles in EXO 2030+375 has also been reported earlier (Reig & Coe 1999; Klochkov et al. 2008; Naik et al. 2013; Naik & Jaisawal

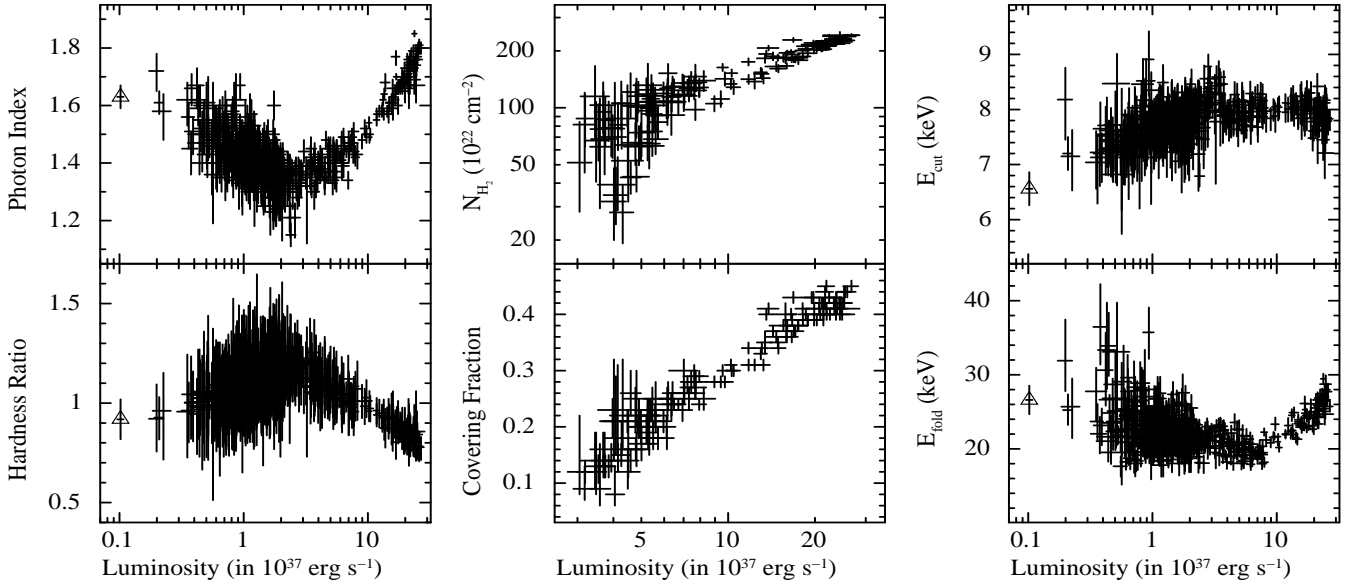


**Figure 6.** Spectral parameters such as photon index (top left panel), additional column density (top middle panel), cutoff energy (top right panel), covering fraction (bottom middle panel) and folding energy (bottom right panel) obtained from the spectral fitting of *RXTE* observations of EXO 2030+375 with a partial covering high energy cutoff power-law model during Type I and Type II outbursts, are shown with the 3-30 keV luminosity. Hardness ratio (ratio between 10-30 keV flux and 3-10 keV flux) with luminosity is also shown in bottom left panel of the figure. The parameters from *NuSTAR* observation are marked with empty triangles. The error bars quoted for  $\sigma$  uncertainties.

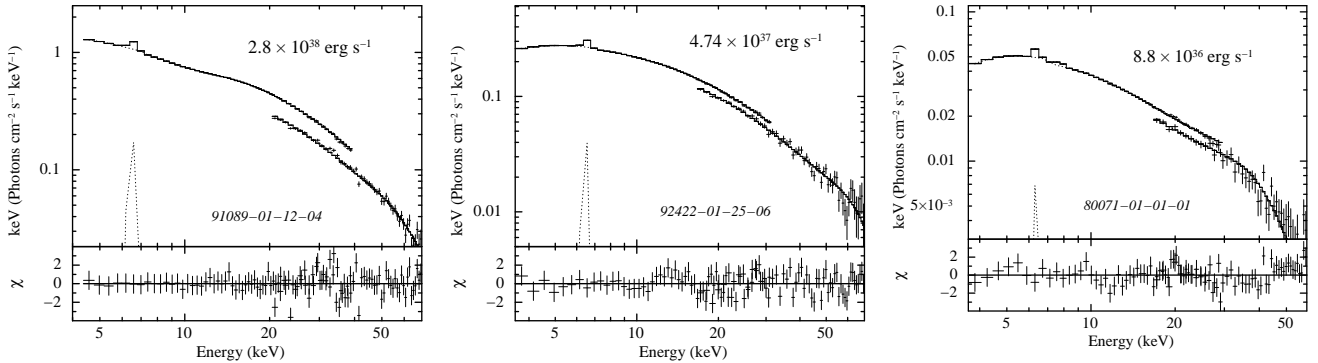


**Figure 7.** Phase-averaged energy spectra of EXO 2030+375 at three distinct luminosities obtained during Type-I and Type-II X-ray outbursts obtained from PCA and HEXTE detectors. The spectra of pulsar was fitted with BW model (Ferrigno et al. 2009) along with an iron line at  $\sim 6.4$  keV and partial covering component (top panel of figure). Corresponding spectral residuals are shown in bottom panels of the figure. Any absorption like feature was not seen in 10–20 keV energy range of the pulsar spectra.

2015). The shape of the pulse profiles of the pulsar is complex due to the presence of multiple peaks/dips in soft X-rays. A single peak profile is generally seen at hard X-rays. Sasaki et al. (2010) modeled the energy resolved pulse profiles during a giant outburst to understand the emission components from the magnetic poles of the pulsar. An asymmetric profile was explained by considering a moderate distortion in the magnetic field, which can locate one of the accretion column at relatively close to the line of sight. The composite emissions from both the poles resulted an asymmetry in the profile due to deformity in the location of columns. *Suzaku* observations of the pulsar during 2007 and 2012 Type I outbursts showed nearly symmetrical profiles along with multiple absorption dips at certain pulse phases (Naik et al. 2013; Naik & Jaisawal

2015). These dips showed strong dependence on energy and luminosity. Presence of additional matter in the form of narrow streams that are phase locked to the pulsar is believed to be the cause of these features in pulse profiles. Such absorption like features are also seen in pulse profiles of other Be/X-ray binary pulsars such as A 0535+262 (Naik et al. 2008), GRO J1008-57 (Naik et al. 2011), and GX 304-1 (Jaisawal, Naik & Epili 2016) during outbursts. During 2007 outburst of EXO 2030+375, these dips were present in the profiles up to  $\sim 70$  keV (Naik et al. 2013). Phase resolved spectroscopy confirmed the presence of additional dense matter at same phases of the profile. In addition to absorption dips, sometimes a narrow and sharp dip-like feature was detected in the pulse profiles at low luminosity (Ferrigno et al. 2016). This feature was interpreted

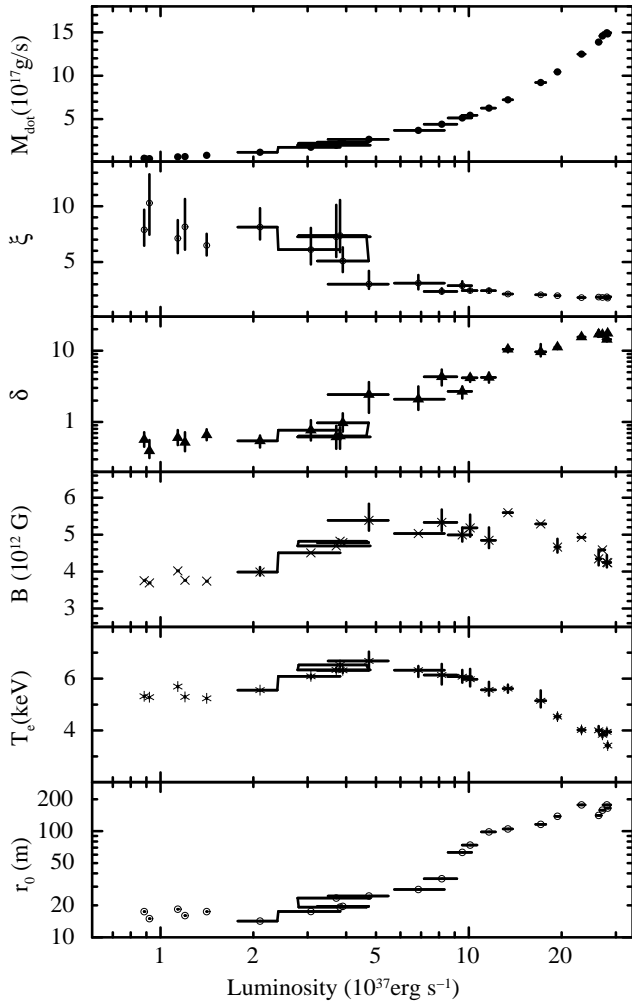


**Figure 8.** Spectral parameters obtained from the fitting of phase averaged spectra of EXO 2030+375 with BW model at different luminosities. The top, second and third panels of figure show the mass accretion rate, diffuse rate, and the ratio of bulk to thermal Comptonization in accretion column, respectively. While the fourth, fifth and sixth panels indicate the luminosity variation of magnetic field, plasma temperature and column radius, respectively.

as due to self absorption from the accretion column. This peculiar feature was also detected in the pulse profiles of EXO 2030+375 and found to be luminosity dependent. The feature was present in the pulse profiles when the pulsar luminosity was below  $4 \times 10^{37}$  erg s $^{-1}$  (critical luminosity regime). It is probable that at lower luminosity, the pencil beam propagating across the magnetic axis interacts with the accretion column directly and produces a dip-like structure in the pulse profile. A significant contribution from fan beam may change the emission geometry and lead to the absence of this feature beyond the critical luminosity, as seen in our study.

## 5.2 Spectroscopy

The broadband energy spectrum of accretion powered X-ray pulsar is known to be originated due to the inverse Comptonization of soft X-ray photons emitted from the hot

spots on the surface (Becker & Wolff 2007). The continuum is generally described with simple models such as high energy cutoff power law, NPEX, exponential cutoff power law etc. despite of the complex phenomenon occurring in the accretion column. A physical model, known as BW model, was also used in our study to understand the spectral properties of the pulsar at different luminosity levels. We carried out spectral analysis of a large number of *RXTE* pointed observations of Be/X-ray binary pulsar EXO 2030+375, spanned over a decade by using a high energy cutoff power-law model along with a partial absorbing component and a Gaussian function for the 6.4 keV iron emission line. The *RXTE* observations of the pulsar provided opportunity to trace spectral evolution of the pulsar at various luminosity levels during Type I and Type II X-ray outbursts since 1996 to 2011. Parameters obtained from the spectral fitting showed very interesting variation with luminosity. The photon index was found to exhibit three distinct patterns with luminosity indicating signatures of spectral transition between sub-critical and super critical states. All three regimes are reflected in the pattern of the pulse profiles and are interpreted as due to different beam pattern at three different luminosity ranges.

A negative correlation was seen between power-law photon index and pulsar luminosity in sub critical regime (below the critical luminosity) where spectrum was relatively hard. In this condition, the broadband X-ray emission is considered to be originated from a hot mount on the neutron star surface (Basko & Sunyaev 1976; Becker et al. 2012). Critical luminosity is associated with the transition between two accretion scenarios. In our study, we detected a plateau like region in the distribution of power-law photon index in luminosity range of  $\sim(2-4) \times 10^{37}$  erg s $^{-1}$ . This luminosity range can be considered as the critical luminosity for EXO 2030+375. The critical luminosity regime has been explored for other accretion powered X-ray pulsars such as 4U 0115+63, V 0332+53, Her X-1, A 0535+26 and GX 304-1 in luminosity range of  $\sim(2-8) \times 10^{37}$  erg s $^{-1}$  (Becker et al. 2012 and reference therein). A positive correlation between photon index and luminosity was detected above the critical luminosity. This occurs because of dominating role of shock in the accretion column which effectively reduces the velocity of energetic electrons. In this case, pulsar spectrum appears soft due to lack of bulk Comptonization of photons with accreting electrons (Becker et al. 2012). A positive correlation between photon index and luminosity, therefore, is observed in super-critical regime. During 1985 giant outburst, the photon index was also proportional to luminosity, indicating that the pulsar was accreting above the critical limit (Reynolds, Parmar & White 1993).

The hardness ratio (ratio between 10-30 keV flux and 3-10 keV flux) also showed similar kind of transition with luminosity. This showed increasing trend till the pulsar luminosity reaches its critical value beyond which a decreasing trend was observed. It showed that the pulsar emission was relatively hard in the sub-critical luminosity region. A softening in the spectrum was observed above the critical luminosity as discussed in above section. The folding energy was found to vary with luminosity. This spectral parameter represents the plasma temperature in the emission region. At lower luminosity, the value of folding energy was relatively constant although a few high values (with large errorbars) were also evident. The high values in sub-critical luminos-

ity regime may correspond to the deep regions of accretion column. The value of folding energy was increasing beyond the critical luminosity. It is expected that increasing mass accretion in super-critical region can produce the high temperature plasma in the presence of shock.

The magnetic field of the pulsar can be investigated by using observed cyclotron resonance scattering features in the broad-band spectrum. Cyclotron resonance scattering features appear due to the resonant scattering of electrons with photons in the presence of magnetic field (Caballero & Wilms 2012). These absorption like features appear in the hard X-ray spectrum of accretion powered X-ray pulsars with magnetic field in the order of  $10^{12}$  G. The detection of these features allow us to directly estimate the magnetic field of pulsar. Detection of a cyclotron absorption line at  $\sim 11$  keV in the pulsar spectrum obtained from *RXTE* observation was reported earlier (Wilson, Finger & Camero-Arranz 2008). Using same data set, we attempted to explore the cyclotron line feature further. However, our results showed that this feature was model dependent, only seen in a single cutoff based model. This discards the detection of cyclotron scattering feature in EXO 2030+375. The feature was also not detected in the pulsar spectra obtained from *NuSTAR* observations, though it was carried out during low intensity phase. Moreover, our studies based on BW model showed a constrain on pulsar magnetic field which is in the range of  $\sim 4-6 \times 10^{12}$  G. For such strength of magnetic field, a cyclotron feature is expected to observed in the 40–60 keV energy range of pulsar spectrum. We have not observed any such features in the above energy range using *RXTE* observations, although a claim of cyclotron line at  $\sim 36$  or 63 keV have been made earlier in the pulsar (Reig & Coe 1999; Klochkov et al. 2008). With high capability of new generation satellite such as *As-trosat* and *NuSTAR*, the cyclotron line feature can be investigated during an intense X-ray outburst.

## 6 SUMMARY AND CONCLUSION

We have carried out a detailed timing and spectral analysis of transient Be/X-ray binary pulsar EXO 2030+375 during several Type I and Type II outbursts during 1996-2011 with *RXTE*. An absorbed power-law modified with a high-energy cutoff along with a partial absorber and a Gaussian component was used to explain the 3-30 keV energy spectrum of the pulsar. The pulse profiles were found to be strongly luminosity dependent at wide range of  $\sim 10^{36-38}$  erg s $^{-1}$ . Observed changes in the shape of pulse profiles are attributed to the change in emission geometry of pulsar. Pulsar emission was dominated by pencil beam at lower luminosity which switched to fan beam at higher luminosity. The different shape of pulse profiles at both the extremes are interpreted as due to different beam patterns. However, a mixture of both patterns are seen in the critical luminosity regime. The profiles were observed to be independent of Type I and Type II outbursts and their phases. Spectral parameters also showed the signatures of emission transition. Based on luminosity, a transition from sub-critical to super-critical regime is seen in the photon index. These changes are explained in terms of changes in the emission geometry across the critical luminosity. At the brighter phases the presence of additional

matter nearby the pulsar is observed due to effect of higher accretion rate. Based on the physical modeling of the continuum spectrum, the magnetic field of pulsar can be estimated to be  $\sim 4-6 \times 10^{12}$  G.

## ACKNOWLEDGMENTS

We thank the referee for his/her constructive suggestions that improved the paper. The research work at Physical Research Laboratory is funded by the Department of Space, Government of India. This research has made use of data obtained through HEASARC Online Service, provided by the NASA/GSFC, in support of NASA High Energy Astrophysics Programs.

## REFERENCES

- Basko M. M., Sunyaev R. A., 1976, MNRAS, 175, 395  
 Becker P. A., Wolff M. T., 2007, ApJ, 654, 435  
 Becker, P. A., Klochkov, D., Schönherr, G., Nishimura, O., Ferrigno, C. et al. 2012, A&A, 544, 123  
 Caballero I., Wilms J., 2012, MmSAI, 83, 230  
 Coe, M. J., Payne, B. J., Longmore, A., & Hanson, C. G. 1988, MNRAS, 232, 865  
 D’Ài A., Cusumano G., Del Santo M., La Parola V., Segreto A., 2017, MNRAS, 470, 2457  
 Ferrigno C., Becker P. A., Segreto A., Mineo T., Santangelo A., 2009, A&A, 498, 825  
 Ferrigno C., Pjanka P., Bozzo E., Klochkov D., Ducci L., Zdziarski A. A., 2016, A&A, 593, A105  
 Fürst F., Wilson-Hodge C. A., Kretschmar P., Kajava J., Kuehnel M., 2016, ATel, 8835,  
 Harrison F. A., et al., 2013, ApJ, 770, 103  
 Jahoda K., Swank J. H., Giles A. B., Stark M. J., Strohmayer T., Zhang W., Morgan E. H., 1996, SPIE, 2808, 59  
 Jahoda K., Markwardt C. B., Radeva Y., Rots A. H., Stark M. J., Swank J. H., Strohmayer T. E., Zhang W., 2006, ApJS, 163, 401  
 Jaisawal G. K., Naik S., Paul B., 2013, ApJ, 779, 54  
 Jaisawal G. K., Naik S., Epili P., 2016, MNRAS, 457, 2749  
 Klochkov D., et al., 2007, A&A, 464, L45  
 Klochkov D., Santangelo A., Staubert R., Ferrigno C., 2008, A&A, 491, 833  
 Kretschmar P., et al., 2016, ATel, 9485,  
 Krimm H., Barthelmy S., Gehrels N., Markwardt C., Palmer D., Sanwal D., Tueller J., 2006, ATel, 861,  
 Levine A. M., Bradt H., Cui W., Jernigan J. G., Morgan E. H., Remillard R., Shirey R. E., Smith D. A., 1996, ApJ, 469, L33  
 Martin R. G., Nixon C., Armitage P. J., Lubow S. H., Price D. J., 2014, ApJ, 790, L34  
 Motch C., Janot-Pacheco E., 1987, A&A, 182, L55  
 Naik S., et al., 2008, ApJ, 672, 516  
 Naik S., Paul B., Kachhara C., Vadawale S. V., 2011, MNRAS, 413, 241  
 Naik S., Maitra C., Jaisawal G. K., Paul B., 2013, ApJ, 764, 158  
 Naik S., Jaisawal G. K., 2015, RAA, 15, 537  
 Negueruela I., Reig P., Coe M. J., Fabregat J., 1998, A&A, 336, 251  
 Okazaki A. T., Hayasaki K., Moritani Y., 2013, PASJ, 65, 41  
 Okazaki A. T., Negueruela I., 2001, A&A, 377, 161  
 Parmar A. N., White N. E., Stella L., Izzo C., Ferri P., 1989a, ApJ, 338, 359  
 Parmar A. N., White N. E., Stella L., 1989b, ApJ, 338, 373  
 Paul B., Naik S., 2011, BASI, 39, 429  
 Reig P., Coe M. J., 1999, MNRAS, 302, 700

- Reig P., 2011, *Ap&SS*, 332, 1  
Reig P., 2008, *A&A*, 489, 725  
Reynolds A. P., Parmar A. N., White N. E., 1993, *ApJ*, 414, 302  
Rothschild R. E., et al., 1998, *ApJ*, 496, 538  
Sasaki M., Klochkov D., Kraus U., Caballero I., Santangelo A.,  
2010, *A&A*, 517, A8  
Stella L., White N. E., Rosner R., 1986, *ApJ*, 308, 669  
Stollberg M. T., 1997, *PhDT*, 2805  
Sun X.-J., Li T.-P., Wu M., Cheng L.-X., 1994, *A&A*, 289, 127  
Wilson C. A., Finger M. H., Coe M. J., Laycock S., Fabregat J.,  
2002, *ApJ*, 570, 287  
Wilson C. A., Fabregat J., Coburn W., 2005, *ApJ*, 620, L99  
Wilson C. A., Finger M. H., Camero-Arranz A., 2008, *ApJ*, 678,  
1263-1272  
Wolf M. T., et al., 2016, *ApJ*, 831, 194